CANADIAN JOURNAL OF EXPLORATION GEOPHYSICS
VOL. 33, NOS. 1 & 2 (DECEMBER 1997), P. 32-45

CONSTRAINED MINIMUM-ENTROPHY DECONVOLUTION

F.K. BOADU[1] AND R.J. BROWN[2]

ABSTRACT

Statistical deconvolution techniques are based upon various assumptions that are incorporated in the operator. When the assumptions are valid, good results may be anticipated. Poor results, on the other hand, may be symptomatic of invalid assumptions. The conventional Wiener spiking deconvolution technique performs very robustly, regardless of the distribution of amplitudes in the reflectivity series, provided the wavelet is minimum-phase or accurately known. Minimum-entropy deconvolution (MED), on the other hand, utilizes the assumption that reflectivity is essentially random and non-Gaussian. These criteria, which are required for optimal performance of either deconvolution technique, are not met in practice for most real seismic data. Often, the wavelet is not sufficiently minimum-phase for spiking deconvolution and the reflectivity series is too nearly Gaussian for MED.

We propose a merger of these two deconvolution techniques, a hybrid optimization procedure termed *constrained minimum-entropy deconvolution* (CMED), that exploits the useful properties of both spiking deconvolution (SD) and MED. CMED can, in many cases, restore proper phase characteristics, suppressing side lobes, while providing sufficient pulse compression. In other words, CMED can potentially overcome the weaknesses of either method used in isolation. By a suitable choice of a weighting factor, CMED can also handle situations where the characteristics of the input data lie close to the optimal performance criteria of either of the two end-member deconvolution methods, SD or MED.

INTRODUCTION

The fundamental objective of seismic deconvolution is to reconstruct the reflectivity series with some resolution by undoing the effects of the propagating source wavelet. Several deconvolution methods have been proposed in the geophysical literature, each with its own optimization criteria and with characteristic assumptions, to compute the filter coefficients.

Conventional deconvolution methods such as spiking deconvolution (SD) or predictive deconvolution (Robinson and Treitel, 1967; 1980) seek to whiten the spectra by imposing restrictions on the phase of the source wavelet to compute the filter coefficients. Minimum-entropy deconvolution (MED) (Wiggins, 1978; Donoho, 1981) attempts to find a linear operator that maximizes the spikiness of the reflectivity, thereby reducing the disorder in the series and hence minimizing entropy. MED does not assume a minimum-phase wavelet and its operator is designed from a multitrace input, selectively suppressing frequency bands over which the ratio of coherent signal to random noise is low.

Real data often violate the assumptions underlying both MED and SD. However, by merging the two techniques through a hybrid optimization scheme, termed: *constrained minimum-entropy deconvolution* (CMED), one may potentially combine the robustness of spiking deconvolution with the insensitivity of MED to the input phase characteristics. The filter coefficients are derived from an optimal combination of conventional spiking deconvolution and the varimax criterion of MED. The optimally derived CMED operator exploits the advantages of the two methods used in isolation for improved performance.

The intent of this note is simply to propose this nonlinear hybrid deconvolution technique as one that could prove to be of practical benefit in certain cases. Our approach at this stage is heuristic or empirical rather than theoretical. Further experimental and theoretical study, as well as algorithmic development, are required.

DECONVOLUTION TECHNIQUES

Spiking deconvolution

Conventional deconvolution techniques assume a model in which the reflectivity is a random and uncorrelated series of events with a white spectrum. The standard approach in computing the prediction-error filters involves the use of the Wiener-Levinson algorithm (Robinson and Treitel, 1967; Peacock and Treitel, 1969) which requires the explicit computation of the input-trace autocorrelation. The spiking operator does a good job in the recovery of the earth impulse

Manuscript received by the Editor March 1, 1997; revised manuscript received March 13, 1997.

[1]Department of Civil and Environmental Engineering, Box 90287, Duke University, Durham, North Carolina 27708-0287 USA

[2]Department of Geology and Geophysics, The University of Calgary, Calgary, Alberta, Canada T2N 1N4. Presently on leave at PGS Reservoir AS, P.O. Box 354, N-1324 Lysaker, Norway.

We would like to thank Dan Hampson for helpful discussion at an early stage of this work, as well as Larry Lines and an anonymous reviewer for constructive criticism of this manuscript. Veritas Seismic Ltd., Calgary, graciously donated the data for the example presented. Bill Matheson provided expert graphics assistance.

response if that response is nearly white, random and stationary, and if the seismic wavelet is minimum-phase or accurately known (Ziolkowski, 1984). Jurkevics and Wiggins (1984) observed that spiking deconvolution is robust under a wide range of reflectivity and signal-distortion conditions and still remains the universal choice in practice. Its successful application, like that of any other statistical deconvolution method, depends on the assumptions made in the development of the deconvolution operator.

Minimum-entropy deconvolution

Minimum-entropy deconvolution (Wiggins, 1978; Ooe and Ulrych, 1979; Donoho, 1981; DeVries and Berkhout 1984; Sacchi et al., 1994) designs the linear operator which, when applied to the seismic trace, leaves behind the smallest number of large spikes consistent with the data. Such an operator is designed by maximizing some data-simplicity measure with respect to the filter coefficients. The measure chosen by Wiggins (1978) is the varimax (or simplicity) norm defined for a multichannel time series **X** as:

$$V(\mathbf{X}) = \sum_{j=1}^{T} \left\{ \sum_{i=1}^{S} x_{ij}^4 \Big/ \left[\sum_{i=1}^{S} x_{ij}^2 \right]^2 \right\} \tag{1}$$

where:

$$\mathbf{X} = \begin{bmatrix} x_{11}\, x_{12} \cdots x_{1T} \\ x_{21}\, x_{22} \cdots x_{2T} \\ \vdots \quad \vdots \quad \ddots \quad \vdots \\ x_{S1}\, x_{S2} \cdots x_{ST} \end{bmatrix} = \left(\mathbf{x}_1, \mathbf{x}_2, \ldots\ldots, \mathbf{x}_T \right) \tag{2}$$

where x_{ij} is the ith sample of the jth trace with S samples and T traces, and $\mathbf{x}_j$ represents the single jth trace.

The varimax norm has the property that, for each trace, it is maximized to $V = 1$ ($V = T$, for T traces) when the trace consists of a single spike of unit amplitude. In general, the more nonzero spikes of consistent amplitude there are, the smaller the varimax becomes. The MED normal equations (Wiggins, 1978), as they stand, are highly nonlinear and, as such, cannot be solved directly. However, they may be solved recursively in a fairly straightforward fashion, which "may not lead to a unique maximum value for V but ... leads to a useful local maximum" (Wiggins, 1978).

Wiggins (1985) noted that MED does not work very well most of the time and discussed a number of reasons for this. He also proposed an alternative deconvolution procedure, "entropy-guided deconvolution", designed to provide suitable deconvolution for real random seismic data and for wavelets of any phase. A feature of this scheme is that it approaches Wiener behavior as the probability distribution of the reflectivity series becomes more Gaussian. Other problems with MED have been dealt with, for example, by Donoho (1981), Jurkevics and Wiggins (1984) and Deeming (1984), chief among them, perhaps, the question of model validity: if the reflectivity series within the design window does not have the minimum-entropy property, i.e., that of a sparse-spike sequence, then applying an MED-designed operator tending to produce such a sparse output would be inappropriate.

Other techniques

Considerable recent theoretical work has been published on higher-order statistics and blind deconvolution (Mendel, 1991; Lacoume, 1992) and the effects on performance of such quantities as kurtosis, bandwidth, and duration (White, 1988; Boumahdi and Glangeaud, 1994), which surely will lead to improvements over such methods as SD and MED. Indeed, the hybrid method presented here, CMED, is not intended to eclipse such new and sophisticated methods. The objectives of this paper are quite limited and specific: to present CMED as one possible deconvolution method that might be appropriate in many cases and which may be fairly readily implemented using software components that are widely available.

Constrained Minimum-Entrophy Deconvolution

Constrained minimum-entropy deconvolution (CMED) is developed for the purpose of combining the useful properties of Wiggins MED and Wiener spiking deconvolution. In real situations we expect the large degree of nonlinearity of the CMED varimax, coupled with the general instability of deconvolution and sensitivity to noise, to yield a "bumpy" objective function, i.e., one with multiple local minima. As mentioned earlier, the constrained varimax functional is complicated and its direct solution is a difficult problem. However, the problem can be solved by using an optimization scheme like that of Rothman (1985) that avoids the local linearization pitfalls of Wiggins's (1978) algorithm and searches for solutions close to the global minimum of the CMED objective function. The resulting algorithm conveniently adjusts to any desired combination of MED and Wiener deconvolution by a suitable choice of weighting factor.

Constrained MED varimax functional

Following from equation (1) and defining the MED filter output as:

$$y_{kj} = \sum_{l=1}^{L} f_l x_{k-l+1,j}, \tag{3}$$

the MED varimax norm may be written as:

$$V(\mathrm{Y}) = \sum_{j=1}^{T} V\left(\mathbf{y}_j\right) = \sum_{j=1}^{J} \left\{ \sum_{k=1}^{K} y_{kj}^4 \Big/ \left[\sum_{k=1}^{K} y_{kj}^2 \right]^2 \right\} \tag{4}$$

where x_{ij} = input signal, K = number of time samples per trace, T = number of traces, and f_l are the L filter coefficients (filter length).

Any approach used to maximize $V(\mathbf{Y})$ will lead to the MED solution. Wiggins (1978) chose the iterative procedure using the Levinson algorithm. The prediction-error operator (spiking operator) can be obtained as a solution to the equation of the form:

$$\sum_{m=1}^{L}\left[f_m\phi_{xx}(l-m)-\phi_{zx}(l)\right]=0 \tag{5}$$

where $\phi_{xx}(\tau)$ is the autocorrelation of the input at lag τ, f_m are the filter coefficients, and $\phi_{zx}(\tau)$ is the crosscorrelation between input and desired output. For multitrace cases, an average autocorrelation is computed for all the traces. Minimization schemes for the solution of equation (5) using the conjugate-gradient and gradient algorithms have been utilized by Wang and Treitel (1973). The approach adopted here is to minimize the sum of squares of the bracketed terms of equation (5).

The constrained-varimax norm $C(\mathbf{Y})$ is then obtained by convex combination of equations (4) and (5), thus:

$$C(\mathbf{Y})=\phi_1(\lambda)\sum_{j=1}^{T}\left\{\sum_{k=1}^{K}y_{kj}^4\Big/\left[\sum_{k=1}^{K}y_{kj}^2\right]^2\right\} \tag{6}$$

$$+\phi_2(\lambda)\sum_{j=1}^{T}\sum_{m=1}^{L}\left[f_m^j\phi_{xx}(l-m)-\phi_{zx}^j(l)\right]^2$$

To ensure convexity: $\phi_1(\lambda)+\phi_2(\lambda)=1$; $\phi_1(\lambda)\geq 0$, and $\phi_2(\lambda)\geq 0$; $\phi_1(\lambda)$ decreasing monotonically on $[0,1]$ and $0\leq\lambda\leq 1$, λ being a weighting factor expressing relative emphasis on either term of equation (6). Heuristically, $\phi_1(\lambda)=1-\lambda^4$ and $\phi_2(\lambda)=\lambda^4$ were chosen simply to be in accord with the exponent 4 in the varimax norm. By adopting such a convex combination, the solution swings from one extreme, say that of spiking deconvolution for λ^4, or λ, equal to unity, to that of MED for λ equal to zero. The CMED solution lies, in general, somewhere between these limits of λ. An average autocorrelation of all the traces was utilized in the computation of the CMED operator. The only unknown parameters in equation (6) are the filter coefficients on which the output is dependent. The solution of the CMED equation lends itself particularly to optimization routines which require function evaluation only.

Optimization approach

Owing to the complexity of the CMED objective function and inadequate knowledge of the optimal filter coefficients, application of direct-search methods (e.g., Box et al., 1969) in the maximization is preferable. The optimization routine chosen, due to Bremermann (1970), is essentially an unconstrained global optimization routine, guaranteed to converge for fourth-order functions (Bremermann and Lam, 1970). At an iteration point $x^{(0)}$, the method generates a random direction vector r (with Gaussian distribution) and determines the restriction of the varimax function C to the line $x^{(0)}+\lambda r$.

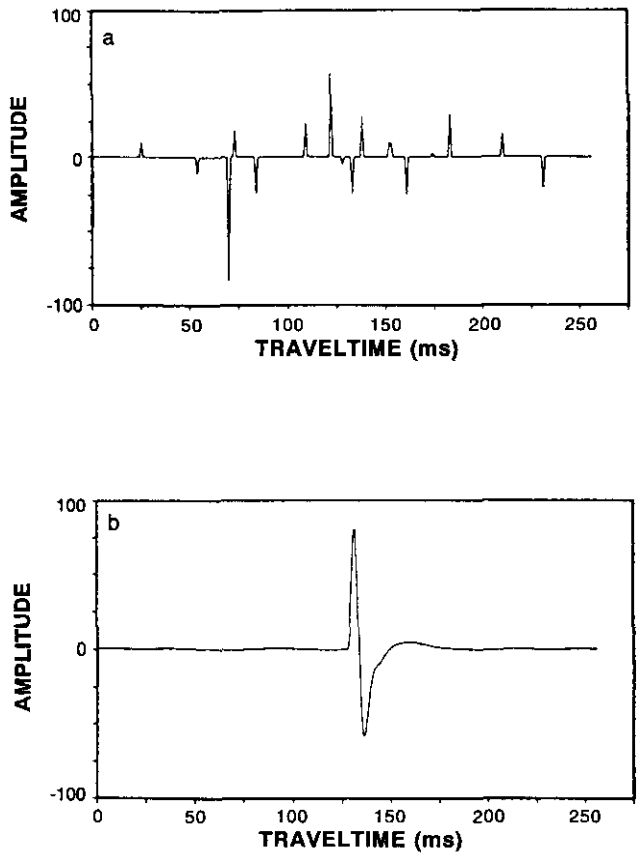

Fig. 1. Input and output after deconvolution (model A): **(a)** sparse reflectivity series, **(b)** minimum-phase source wavelet.

This restriction is a fourth-order polynomial in the parameter λ, whose coefficients are determined by five-point Lagrangian interpolation. The derivative is a third-order polynomial which has either one or three real roots. These roots are computed by Cardan's formula (Bremermann, 1970).

If there is one root, λ_0, the procedure is iterated from the point with a new random direction, provided $C(x^{(0)}+\lambda_0 r)\leq C(x^{(0)})$. If this inequality does not hold, the method is iterated from $x^{(0)}$ with a new random direction. When there are three roots, λ_1, λ_2, λ_3, then the functional is evaluated at $x^{(0)}+\lambda_1 r$, $x^{(0)}+\lambda_2 r$, and $x^{(0)}+\lambda_3 r$. The procedure is iterated from the point where the value of C is minimum, continuing until a predetermined number of iterations have been run or C has decreased to a prescribed value. The initial guess need not be close to the optimum filter values, though a closer guess implies fewer iterations to the optimum.

The convergence properties of the method have been analyzed by Bremermann (1970). And, in a comparative assessment of five least-squares inversion methods, Hoversten et al. (1982) noted that for Bremermann's method the number of function evaluations used in the iterative procedure is independent of the number of parameters (filter coefficients) describing the system, while the other four routines (ridge regression, spiral algorithm, Peckam's method, simplex

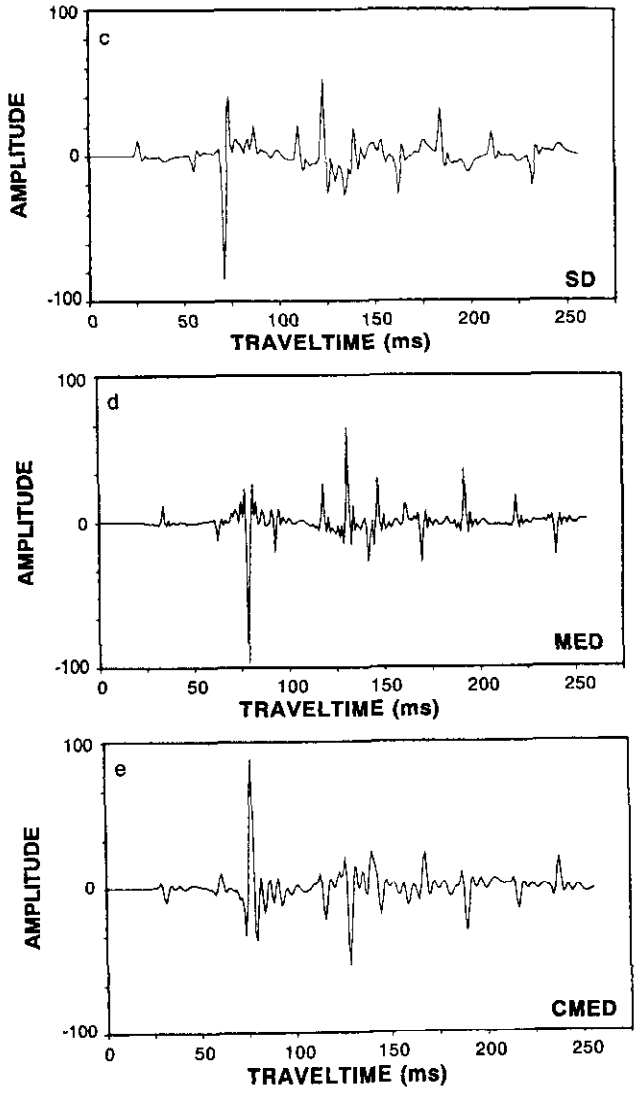

Fig. 1. (c) output after applying SD, **(d)** output after applying MED, **(e)** output after applying CMED.

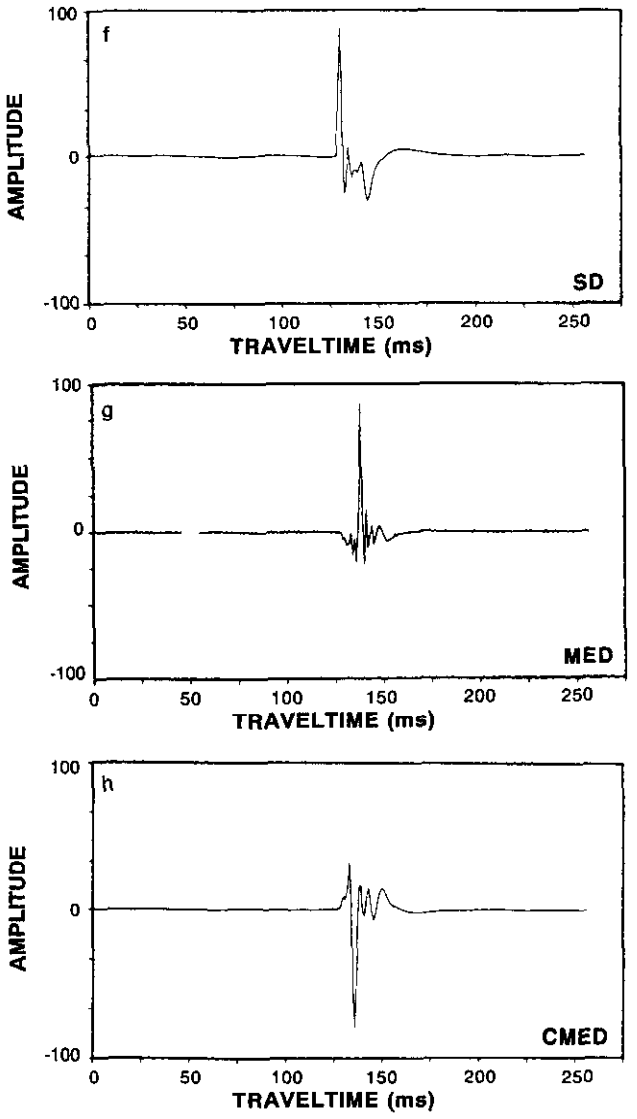

Fig. 1. (f) residual wavelet after SD, **(g)** residual wavelet after MED, **(h)** residual wavelet after CMED. Amplitudes in all figures are arbitrarily normalized to [–100%, 100%].

method) require more function evaluations as the number of parameters increases.

In the design of the CMED algorithm, the approach taken is to use the direct-search (global optimization) routine due to Bremermann (1970) to investigate the constrained varimax norm over some broad region of interest by a predetermined number of iterations, usually 10 to 30. At this stage, the parameters constitute a good initial guess for local optimization for faster convergence and efficient investigation. The output of the local optimization routine after successful convergence is the CMED operator. In most of the successful runs, 300 to 400 iterations were carried out.

As can be seen from equation (6), the CMED norm has the weighting factor as an input parameter. As will be seen later, the phase-resolution characteristics of the propagating wavelet are dependent on this parameter. A user-friendly algorithm developed for CMED allows for flexible input of the weighting factor, choice of the design window, and heuristic estimation of filter length.

Evaluation of CMED Performance

The performance criterion for the three deconvolution methods was established following the procedure by Jurkevics and Wiggins (1984). Synthetic data with known reflectivities and wavelets were deconvolved using all three techniques. The degree of pulse compression was assessed by a residual wavelet, a measure of average waveform remaining in the seismogram after deconvolution. This measure was utilized by Jurkevics and Wiggins (1984) in their critique of seismic deconvolution methods and we deem it satisfactory for purposes of this paper. This residual wavelet is defined in the frequency domain by division as:

$$\text{residual wavelet}\ (\omega) = \frac{\text{processed output}\ (\omega)}{\text{true reflectivity}\ (\omega)} \qquad (7)$$

and, in practice, a small constant (white noise) can be added to the denominator to avoid instabilities caused by division by very small numbers.

For ideal deconvolution, the time-domain residual would be a spike, i.e.: output = reflectivity. And the residual for no deconvolution would be the original source wavelet, i.e.: output = input. In real situations, the residual resides between the two extremes. Any phase distortions introduced in the propagating wavelet can be discerned by examining the output residual wavelet. Thus the residual wavelet is a good indicator of the degree of pulse compression and phase distortion or restoration.

Synthetic data results

A comparative study was performed on the three methods, SD, MED and CMED. The synthetic data contain different source wavelets: minimum-phase, band-limited zero-phase and band-limited phase-shifted (90°) wavelets. We used sparse and dense reflectivities that were thought to simulate well a variety of field conditions. The three methods were applied to the input traces and the outputs examined. In most cases the residual wavelet was examined as it gave a good indication of the performance of the particular deconvolution method in question. Several models that included different distributions of reflectivity and different source wavelets were run (Boadu, 1987) and we here present a few examples of the most relevant results.

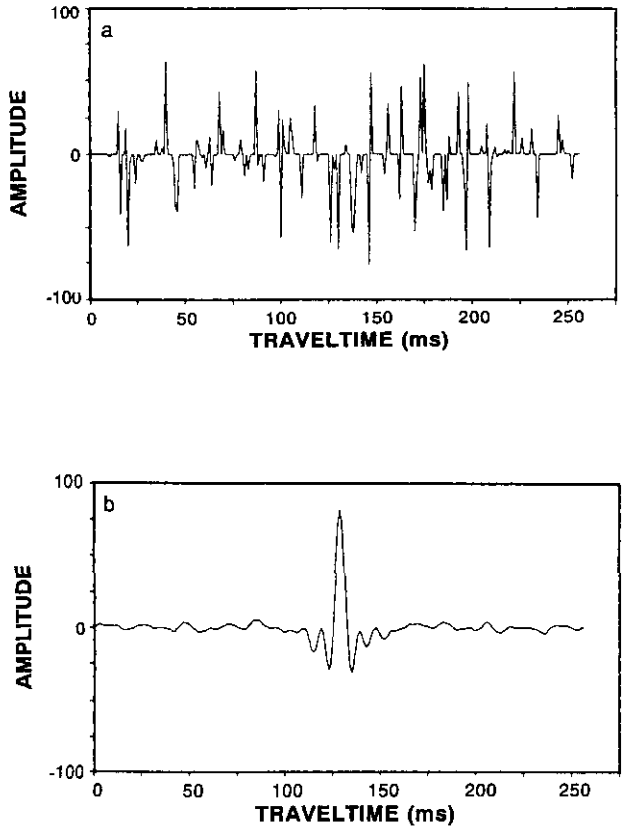

Fig. 2. Input and output after deconvolution (model B1): **(a)** dense reflectivity series, **(b)** band-limited zero-phase source wavelet.

Example 1, model A1. – Model A1 consists of a sparse reflectivity series (Fig. 1a) convolved with a minimum-phase source wavelet (Fig. 1b). Outputs after deconvolution using the three methods are illustrated in Figures 1c, d, and e. Each method does a reasonable job of compressing the source wavelet and reproducing the original reflectivity. MED gave the best result, as the characteristics of the input model were consistent with the assumptions made in obtaining the MED operator. The residual wavelets extracted after deconvolution are shown in Figures 1f, g, and h. Suppression of side-lobes is a desirable characteristic in situations where phase resolution is vital, as in high-resolution seismic and in the exploration for stratigraphic traps (e.g., Rietsch, 1982), and in this case MED and CMED do a better job than SD.

A symmetric filter (Wiggins, 1978) of length 16 points was used as the initial guess in both MED and CMED, with a weighting factor of 0.05. The CMED residual wavelet shows lower frequencies as well as a polarity reversal. The lower

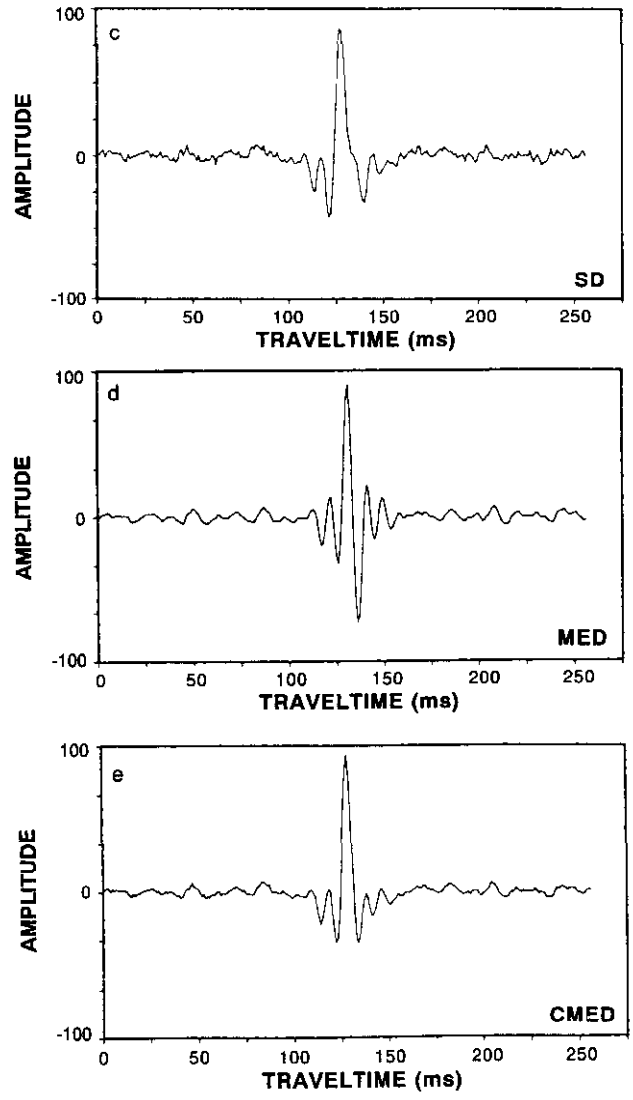

Fig. 2. (c) residual wavelet after SD, **(d)** residual wavelet after MED, **(e)** residual wavelet after CMED.

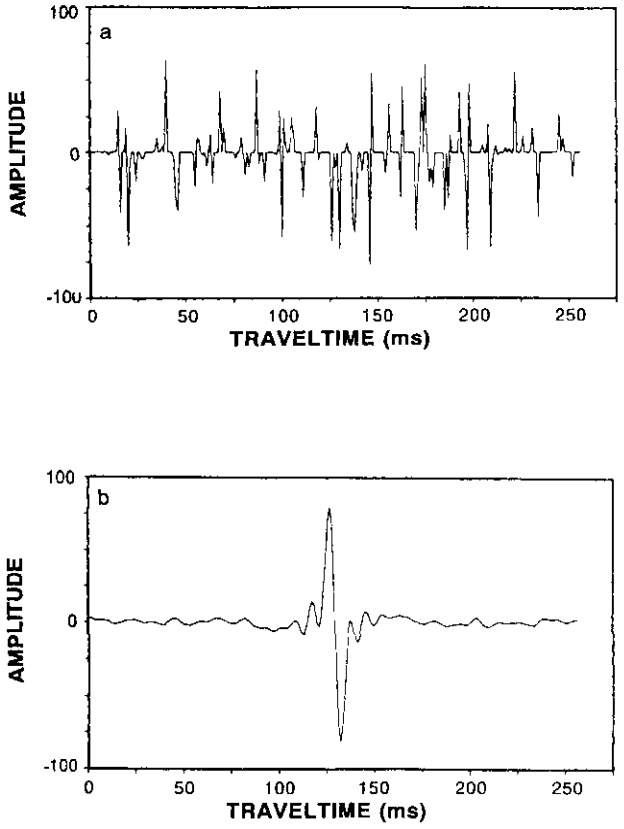

Fig. 3. Input and output after deconvolution (model B2): **(a)** dense reflectivity series, **(b)** 90° – phase-shifted source wavelet.

frequencies may be attributable to the nature of the objective function used in the CMED algorithm. The combination of the fourth-order varimax functional and the second-order autocorrelation tends to reduce both numerical instabilities and the estimation variance, contributing to the robustness of CMED. The time delay observed in both MED and CMED is likely due to the filter length chosen. This may pose a potential problem for the two methods. However the problem is partly solved by trial runs to determine the filter length that maximizes and tapers the objective functions.

The polarity reversal seen is characteristic of MED-like norms: i.e., that the polarity of the output "spikes" cannot be predicted as they do not affect the maximization of the varimax norm (Wiggins, 1978). (Compare, for example, Figs. 5b and 7b.) In general, the output will appear reversed if, on average, negative lobes are larger than positive ones. Wiggins (1978) suggests applying a polarity reversal to outputs after careful comparison of outputs and inputs.

Example 2, model B1. – Model B1 is a dense reflectivity series (Fig. 2a) convolved with a band-limited zero-phase wavelet shown in Figure 2b. The nature of this reflectivity series simulates very well real data situations with reflectors occurring, on average, about every 4.5 ms (Jain, 1986). The wavelet is of a trapezoidal passband of 12 Hz to 55 Hz, with taper zones from 8 to 12 Hz and 55 to 65 Hz. This frequency

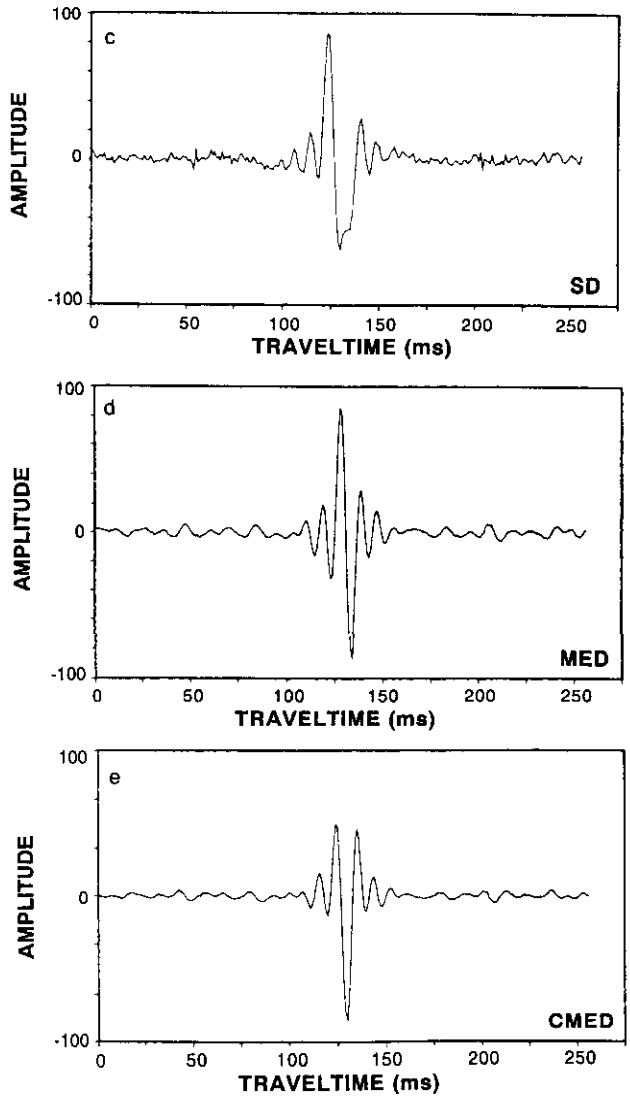

Fig. 3. (c) residual wavelet after SD, **(d)** residual wavelet after MED, **(e)** residual wavelet after CMED.

band has been reported by Jain (1986) as representative of much data collected in Alberta over the last several years. This test wavelet is somewhat noisy because it was band-pass-filtered in order that its frequency content should match that specified.

Figures 2c, d, and e show the residual wavelets after processing with the three methods. The SD residual wavelet is a reasonable representation of the source wavelet; however, the CMED residual wavelet (weighting factor of 0.35) is significantly better and appears the best (the most spike-like) of the three. Side lobes are fairly well suppressed and there is considerable pulse compression. The MED residual wavelet, the worst of the three, is phase-distorted and unstable.

Example 3, model B2. – This model consists of a dense reflectivity series convolved with a phase-shifted wavelet (Figs. 3a and b). The residual wavelet was examined after application of each of the three methods. Figures 3c, d, and e

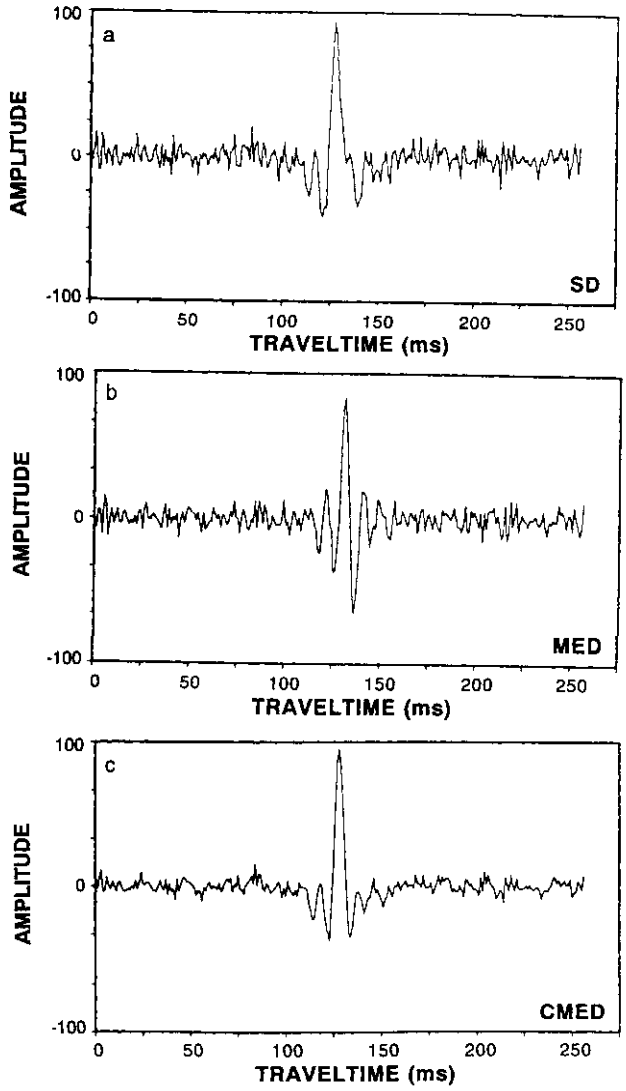

Fig. 4. Residual wavelet after deconvolution of input data (model B1) with 5% white noise added: **(a)** SD, **(b)** MED, **(c)** CMED.

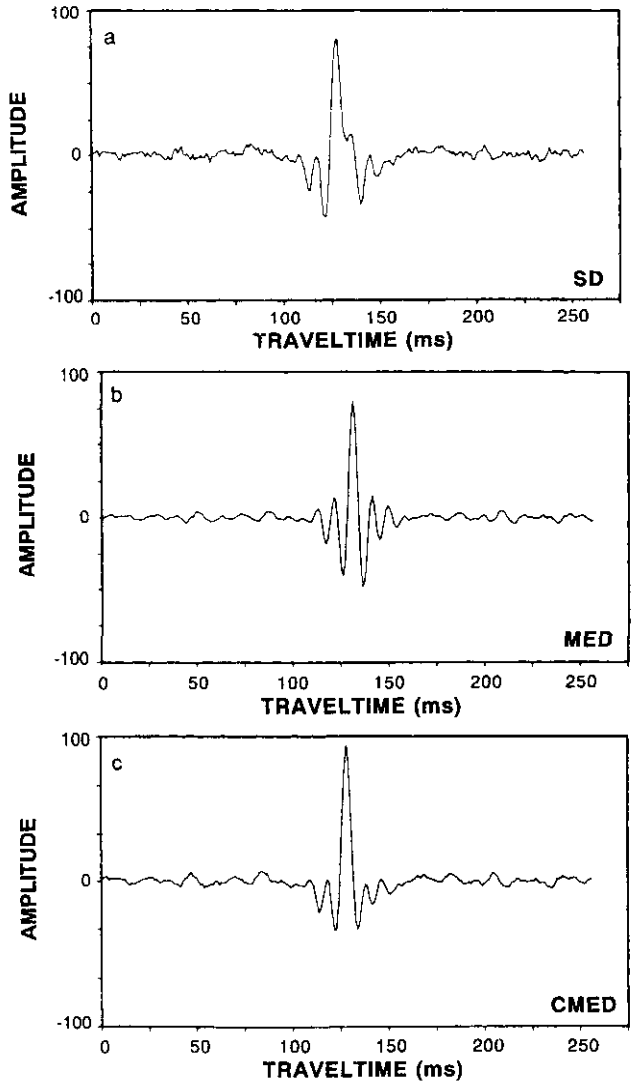

Fig. 5. Residual wavelet, using 5-point filter, after: **(a)** SD, **(b)** MED, **(c)** CMED.

are the outputs of the residual wavelets. A filter length of 8 points was used with a weighting factor of 0.12 for the CMED. The CMED provides a better and cleaner residual wavelet with reasonable suppression of sidelobes, whereas the MED and SD residual wavelets show considerable phase distortion.

Effects of noise

Noise of any form degrades most inversion or deconvolution processes as it leaves stratigraphic imprints unclear. Berkhout (1977) indicated that even low-level noise is detrimental to reliable wavelet deconvolution using a one-sided operator. Any procedure which attempts to suppress noise or reduce amplification of noise is thus desirable. Figure 4 shows residual wavelets after processing using the three deconvolution methods. The input model is Model B1 with additive noise (5% white noise). This random noise is of uniform distribution with the maximum amplitude as a percentage of the largest signal amplitude.

We observe that the CMED (Fig. 4c) has done the best job in terms of reducing noise amplification. The average waveform after SD has the highest noise level. Waveform distortion is seen in the MED residual wavelet.

Effect of filter length on CMED output

As previously mentioned the length of the deconvolution operator is often a sensitive parameter in MED-like deconvolution schemes. Figures 5, 6, and 7 show the residual wavelets after processing of Model Bl with 5-point, 20-point, and 30-point filters, respectively. In Figure 5, each method shows adequate pulse compression and sufficient side-lobe suppression, the best 5-point result being for CMED. In the 20-point case (Fig. 6) the pulses are generally worse, being

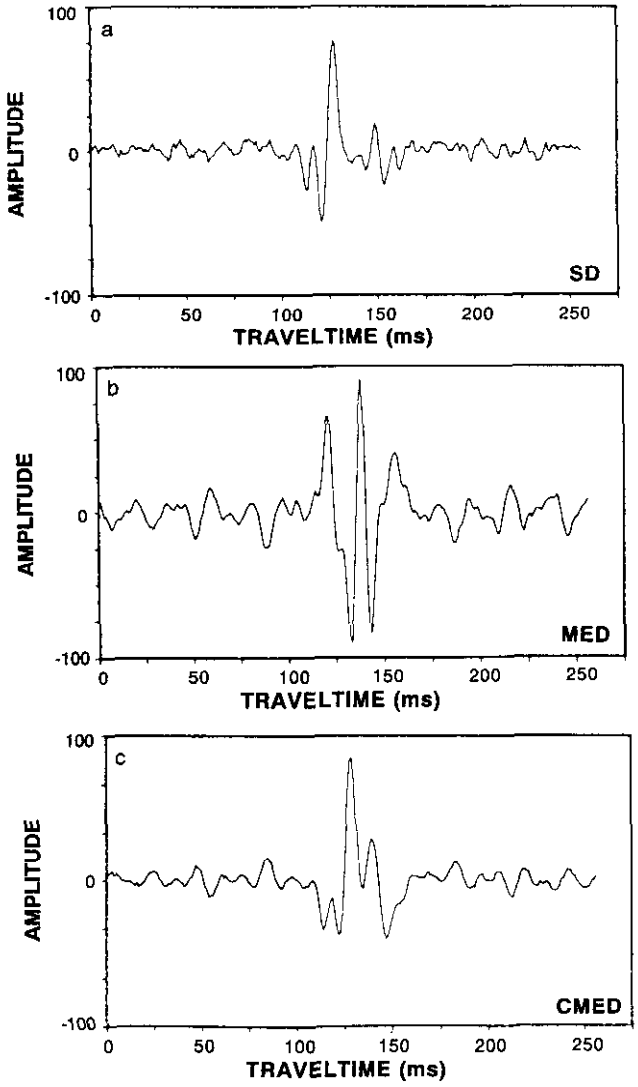

Fig. 6. Residual wavelet, using 20-point filter, after: **(a)** SD, **(b)** MED, **(c)** CMED.

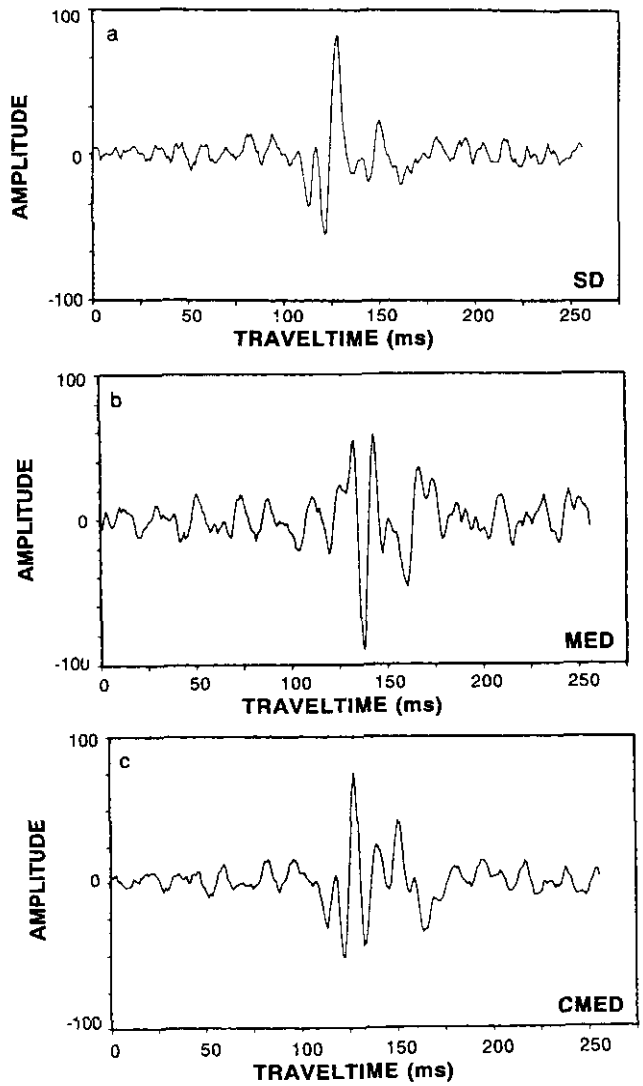

Fig. 7. Residual wavelet, using 30-point filter, after: **(a)** SD, **(b)** MED, **(c)** CMED.

broader than for the 5-point case (Fig. 5). In this case, CMED and SD are about equally good, MED being worst. In Figure 7, the continuing degradation of output with filter length is clearly seen. One may also observe that SD is not nearly as sensitive to filter length as MED or CMED is. Better results are obtained from CMED using shorter filter lengths.

Effects of weighting factor on CMED output

In the design of the CMED operator, a weighting factor in the form of a parameter is introduced in the CMED objective fimction. A suitable choice of this parameter allows the solution to swing from SD to MED. Figure 8 shows the residual wavelet outputs (Model B1) varying the weighing factor, values being 0.3, 0.35, and 0.4. The gradual shift in phase with the weighting factor can be seen. An optimum value of 0.35 sets the phase close to zero. The weighting factor is thus a critical parameter in phase selection. By examining output for various values of the weighting factor, one can find a reasonable value. The choice of the weighting factor at present is heuristic. However, a more appropriate way is to include the weighting factor as a parameter to be estimated by optimization of the CMED objective functional.

Amplitude spectra

Figure 9 shows one example of amplitude spectra before and after deconvolution of noisy input data (Model B1 corrupted with 5% noise). The noise dominates in the high-frequency portion of the spectrum as incoherent signal. SD blows up these incoherent signals considerably. MED reduces signal amplitude in low-frequency portions of the spectrum and boosts, to a lesser extent, the high-frequency incoherent signals. CMED (Fig. 9c) amplifies some of the low-frequency signal and, relative to SD and MED suppresses

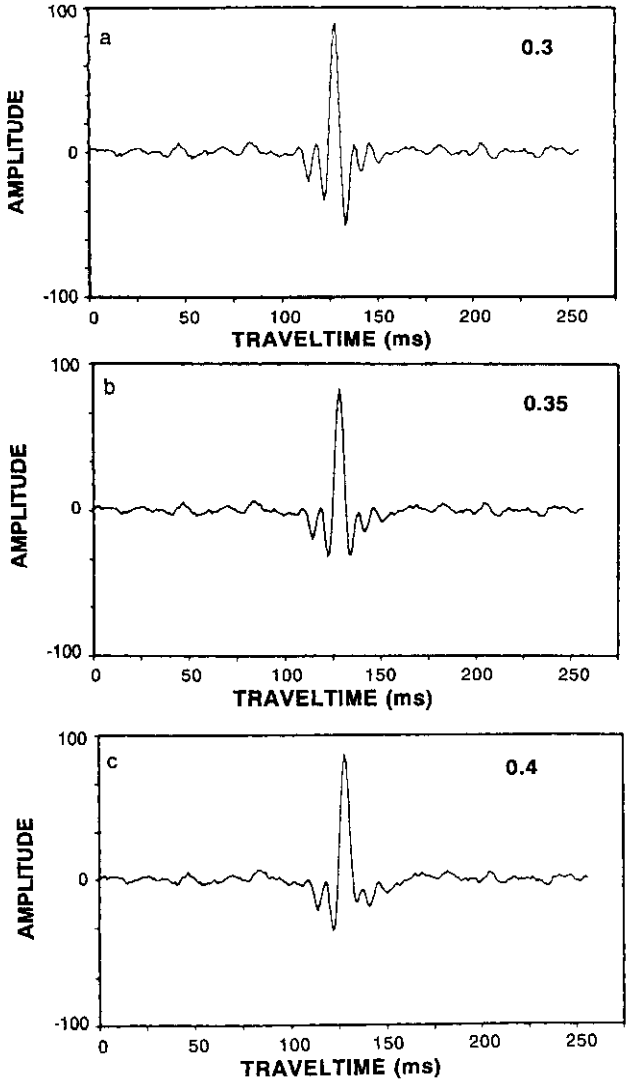

Fig. 8. Effect of varying the weighting factor (CMED) on phase of the residual wavelet: **(a)** 0.3, **(b)** 0.35, **(c)** 0.4.

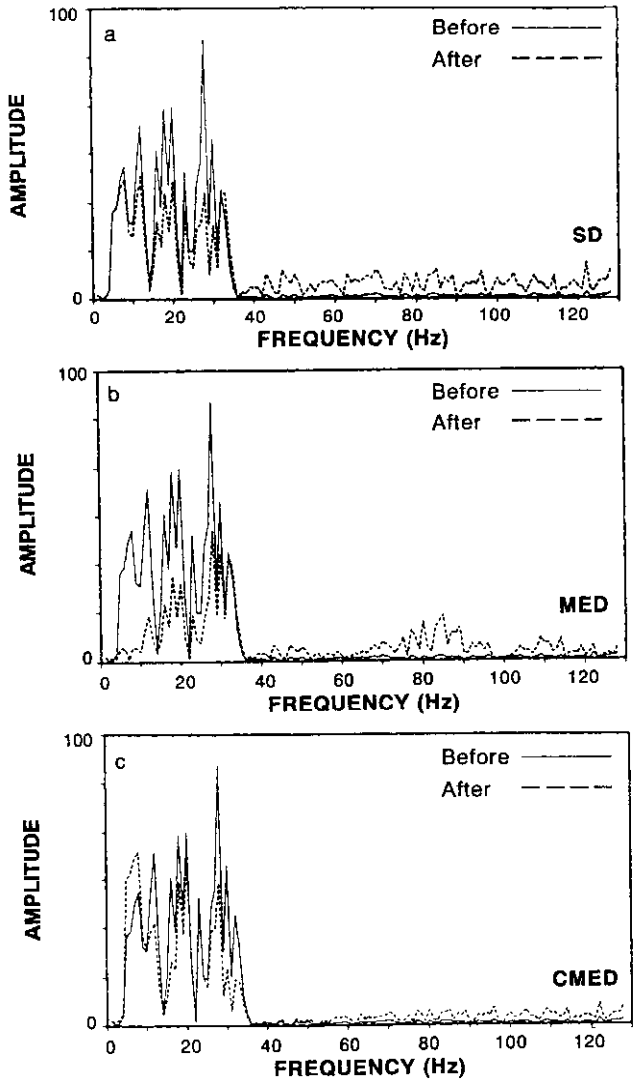

Fig. 9. Amplitude spectra before and after deconvolution (5% noise) for: **(a)** SD, **(b)** MED, **(c)** CMED.

the high-frequency incoherent signals. Again, this property of CMED is advantageous as amplification of such high-frequency noise may become a problem, particularly at late reflection times. Such noise may also cause serious errors in phase treatment produced by spiking deconvolution (Berkhout, 1977).

Real data

A field shot record obtained from Veritas Seismic Ltd. (Calgary) was used to test the performance of CMED on real data. Figure 10a shows the unprocessed data. Figures 10b, c, and d show the processed data using SD, MED and CMED, respectively. The deconvolution parameters for the spiking deconvolution were: an operator length of 22 points, a white-noise level of 0.5%, and a design window of length between 400 and 650 ms. The MED was processed with an operator length of 22 points while the CMED had a filter length of 22 points and a weighting factor of 0.1.

Some improvements of the CMED over the other two methods can be discerned from the gathers. The reflectors have been clearly isolated with better resolution and signal-to-noise ratio. The main reflectors which exhibit some doublets in the MED and SD sections show as single events on the CMED sections.

Applicability of CMED

One of the prime aims of most standard deconvolution techniques is to produce a common-midpoint (CMP) stacked section in which each trace can be considered as the earth's primary reflectivity series convolved with a zero-phase wavelet. We thus expect the residual wavelet to be zero-phase, though more often it is not. The variety of reasons which give rise to this phase distortion have been described by Levy and Oldenburg (1982). Stability of phase becomes

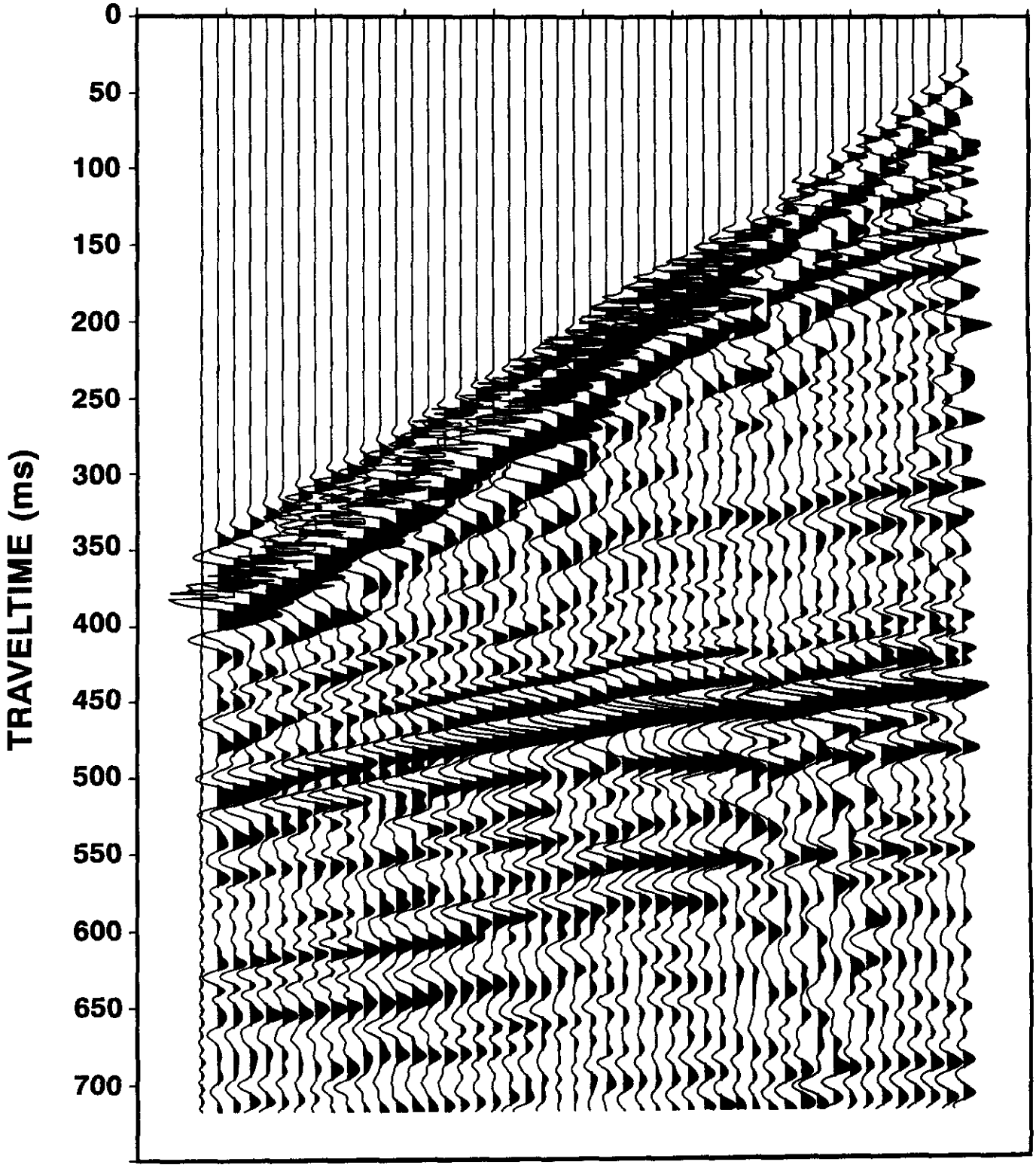

Fig. 10. Real data example: **(a)** unprocessed data.

important when looking for stratigraphic traps, whose detection is dependent on local changes in lithology. These detailed changes in lithology are expressed on the processed section as lateral changes in amplitude and phase of the earth's reflectivity. In seismic inversion procedures, slight phase differences between the source wavelet and the residual wavelet can cause small time shifts between inverted traces and sonic logs and can introduce some inaccuracies in inversion results in the vicinity of large velocity contrasts (Jain, 1986).

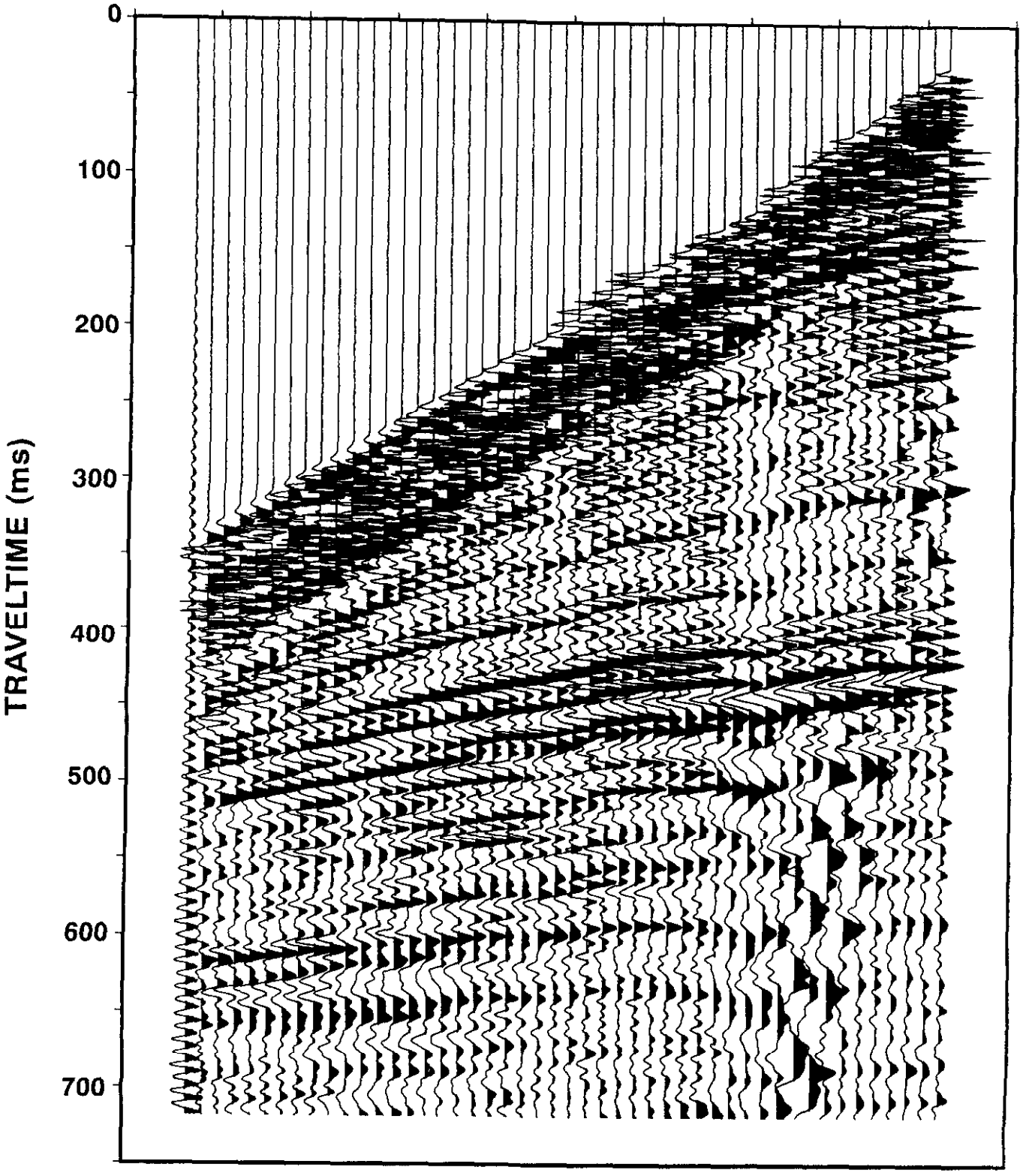

Fig. 10. Real data example: **(b)** processed data (SD).

A common technique to correct for residual phase of the wavelet is to phase shift a number of seismograms in the vicinity of a well until the best match between the synthetic seismogram and the phase-shifted data is found. As commented by Levy and Oldenburg (1987), the mathematical model of constant phase shift may not be appropriate in all instances. The CMED adopts a simple approach of phase shifting the residual phase to be zero by varying the weighting factor. Usually two or three trials give the required results. For the models run, the

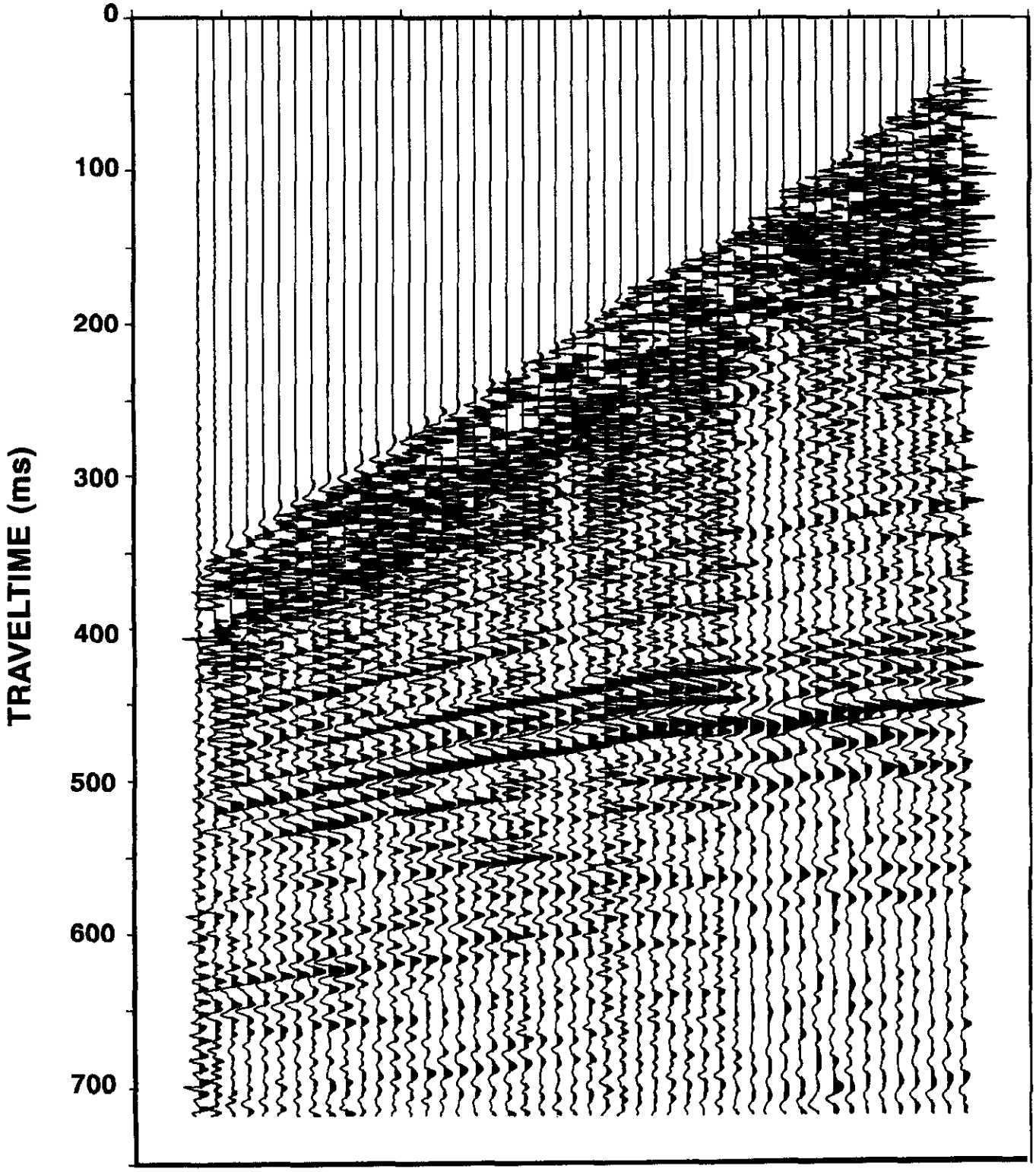

Fig. 10. Real data example: **(c)** processed data (MED).

CMED has the property of stabilizing the residual wavelet, reducing sidelobes and eliminating residual phase.

Suppression of side lobes is very important in enhancing reflection events. Rietsch (1982) favors designing deconvolution filters that place more emphasis on the reduction of side lobes of the filtered wavelet than on sharpening of the deconvolved pulse for normal sampling rate. An appealing feature of CMED is its apparently greater tendency to reduce side lobes.

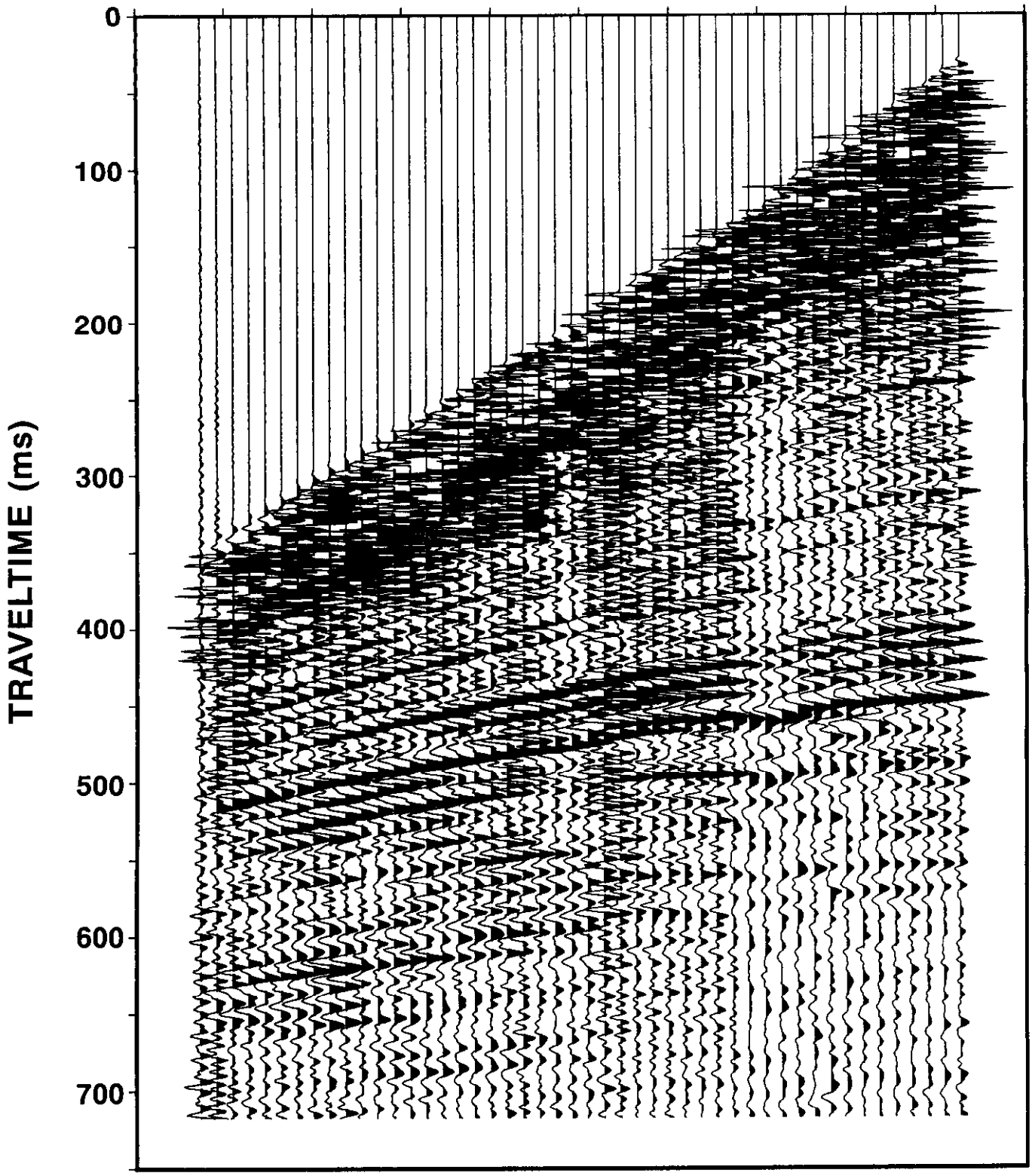

Fig. 10. Real data example: **(d)** processed data (CMED).

Conclusions

A hybrid technique of seismic deconvolution termed constrained minimum-entropy deconvolution (CMED) has been proposed as a combination of spiking and minimum-entropy deconvolution. Outputs from the synthetic data models run using the three deconvolution methods, were compared. The conclusion drawn is that CMED can do a better job in some situations where either MED or SD performs badly. CMED works reasonably well on the real data presented in this

paper. More real data sets are needed for testing to establish the potential of the CMED.

CMED can correct phase errors with a suitable choice of a weighting factor incorporated in the CMED algorithm. In general, shorter filter lengths give better performance. CMED seems to suppress side lobes and increases the signal-to-noise ratio. In particular, it suppresses frequency bands with low signal-to-noise ratio and boosts those bands in which coherent signals dominate. The noise-reduction characteristics of CMED also appear to be positive in the examples shown. In cases where either MED or SD fails to reduce the noise amplifications, the CMED does a relatively good job.

For future work, further processing should be carried out on real data examples. Initially, test panels can be run to determine heuristically the best choice of parameters. However, the optimization process to determine filter parameters over particular zones of interest could perhaps be automated by including these parameters as variables to be determined computationally in the objective function.

Finally, CMED will certainly not universally and perfectly solve the age-old problems of seismic deconvolution. However, it seems to perform better in some situations where the existing or conventional methods fail to provide satisfactory results.

REFERENCES

Berkhout, A.J., 1977, Least-squares inverse filtering and wavelet deconvolution: Geophysics **42**, 1369-1383.

Boadu, F.K., 1987, Constrained minimum-entropy deconvolution: M.Sc. Thesis, The University of Calgary.

Boumahdi, M. and Glangeaud, F., 1994, Nonminimum-phase blind deconvolution: Parametric approach: 64th Annual International Meeting, SEG, Expanded Abstracts, 1595-1598.

Box, M.J., Davis, D. and Swan, W.H., 1969, Non-linear optimization techniques: ICI Monograph. 5, Edinburgh and London.

Bremermann, H.J., 1970, A method of unconstrained global optimization: Mathematical Bioscience **9**, 1-15.

Bremermann, H.J. and Lam, L.S., 1970, Analysis of spectra with non-linear superposition: Mathematical Bioscience **8**, 449-460.

Deeming, T.J., 1984, Why minimum entropy deconvolution doesn't work: SEG Deconvolution Workshop, July 1984, Vail, Colorado.

DeVries, D. and Berkhout, A.J., 1984, Velocity analysis based on minimum entropy: Geophysics **49**, 2132-2142.

Donoho, D., 1981, On minimum entropy deconvolution, *in* Findley, D.F., Ed., Applied Time-Series Analysis II: Academic Press, Inc.

Hoversten, G.M., Dey, A. and Morrison, H.F., 1982, Comparison of five least-squares inversion techniques in resistivity sounding: Geophysical Prospecting 30, 688-715.

Jain, S., 1986, Suitable environments for inversion techniques: a model study: Journal of the Canadian Society of Exploration Geophysicists **22**, 7-16.

Jurkevics, A. and Wiggins, R., 1984, A critique of seismic deconvolution methods: Geophysics **49**, 2109-2116.

Lacoume, J.L., ed., 1992, Higher order statistics: Elsevier Scientific Publishing B.V., 352 p.

Levy, S. and Oldenburg, D.W., 1982, The deconvolution of phase-shifted wavelets: Geophysics **47**,1285-1294.

Levy, S. and Oldenburg, D.W., 1987, Automatic phase correction of common-midpoint stacked data: Geophysics **52**, 51-59.

Mendel, J.M., 1991, Tutorial on higher-order statistics (spectra) in signal processing and system theory: Theoretical results and some applications: Proceedings of the IEEE **79**, 278-305.

Ooe, M. and Ulrych, T.J., 1979, Minimum entropy deconvolution with an exponential transformation: Geophysical Prospecting **27**, 458-473.

Peacock, K.L. and Treitel, S., 1969, Predictive deconvolution: Theory and practice: Geophysics **34**, 155-169.

Rietsch, E., 1982, Deconvolution in the presence of noise and a higher than Nyquist signal rate: Geoexploration **20**, 61-73.

Robinson, E.A. and Treitel, S., 1967, Principles of digital Wiener filtering: Geophysical Prospecting **15**, 311-333.

Robinson, E.A. and Treitel, S., 1980, Geophysical Signal Analysis: Prentice-Hall, Inc.

Rothman, D.H., 1985, Nonlinear inversion, statistical mechanics, and residual statics estimation: Geophysics **50**, 2784-2796.

Sacchi, M.D., Velis, D.R. and Cominguez, A.H., 1994, Minimum entropy deconvolution with frequency-domain constraints: Geophysics **59**, 938-945.

Wang, R.J. and Treitel, S., 1973, The determination of digital Wiener filters by means of gradient methods: Geophysics **38**, 310-326.

White, R.E., 1988, Maximum kurtosis phase correction: Geophysical Journal International **95**, 371-389.

Wiggins, R.A., 1978, Minimum entropy deconvolution: Geoexploration **16**, 21-35.

Wiggins, R.A., 1985, Entropy-guided deconvolution: Geophysics **50**, 2720-2726.

Ziolkowski, A., 1984, Deconvolution: IHRDC Press.